C. R. Mecanique 342 (2014) 425–436

Contents lists available at ScienceDirect

Comptes Rendus Mecanique

www.sciencedirect.com

Separation flow control

Open and closed-loop control of transonic buffet on 3D turbulent wings using fluidic devices

Julien Dandois *, Arnaud Lepage, Jean-Bernard Dor, Pascal Molton, Frédéric Ternoy, Arnaud Geeraert, Vincent Brunet, Éric Coustols

ONERA – The French Aerospace Lab, 8, rue des Vertugadins, 92190 Meudon, France

ARTICLE INFO

Article history:
Received 30 August 2013
Accepted 16 January 2014
Available online 11 June 2014

Keywords:
Transonic
Buffet
Separation control
Vortex generator
Fluidic control
Closed-loop control

ABSTRACT

This paper presents an overview of the work performed recently at ONERA on the control of the buffet phenomenon. This aerodynamic instability induces strong wall pressure fluctuations and as such limits aircraft envelope; consequently, it is interesting to try to delay its onset, in order to enlarge aircraft flight envelop, but also to provide more flexibility during the design phase. Several types of flow control have been investigated, either passive (mechanical vortex generators) or active (fluidic VGs, fluidic trailing-edge device (TED)). It is shown than mechanical and fluidic VGs are able to delay buffet onset in the angle-of-attack domain by suppressing the separation downstream of the shock. The effect of the fluidic TED is different, the separation is not suppressed, but the rear wing loading is increased and consequently the buffet onset is not delayed to higher angles of attack, but only to higher lift coefficient. Then, a closed loop control methodology based on a quasi-static approach is defined and several architectures are tested for various parameters such as the input signal, the objective function or, the tuning of the feedback gain. All closed loop methods are implemented on a dSPACE device calculating in real time the fluidic actuators command from the unsteady pressure sensors data.

1. Introduction

The shock-wave/boundary layer interaction on the upper side of a wing at high Mach number and/or high angle of attack induces a massive flow separation, which can lead to instability. This phenomenon is a global flow instability known as “buffet” and can further lead to structural vibrations called “buffeting”. Buffet results in lift and drag variations that greatly affect the aircraft aerodynamics and, as such, limit the aircraft flight envelope, since a margin of 30% on the lift coefficient at cruising conditions must be respected by design standards. During the last six years, a structured multi-disciplinary research program has been defined at ONERA, which aims at controlling in a closed-loop manner the buffet on 3D wings. This research program had comprised very detailed complementary experimental and numerical studies. Two complementary devices/technologies have been developed for buffet control:

* Corresponding author at: ONERA, DAAP, 8, rue des Vertugadins, 92190 Meudon, France.
E-mail address: julien.dandois@onera.fr (J. Dandois).

http://dx.doi.org/10.1016/j.crme.2014.01.015
1631-0721/

Fig. 1. Experimental set-up in the S3Ch wind tunnel.

- either a fluidic VG (Vortex Generators) actuators, the effect of which is to add momentum and kinetic energy to the turbulent boundary layer that develops upstream of the shock in order to suppress, or at least to delay, the appearance of separated unsteady zones, which are at the origin of the buffet phenomenon;
- or a fluidic TED (Trailing Edge Device/Deflector) actuator, which behaves as a cambered trailing edge by increasing the rear loading of an aerofoil and then postponing the buffet onset at a higher lift coefficient.

At the beginning of 2007, a new joint ONERA research project called "BUFET'N Co" was launched, aimed at controlling buffet studies on 3D turbulent wings [1]. The focus was to investigate buffet control via the use of fluidic devices, which should be easier to handle than mechanical TEDs for closed-loop control applications. In parallel to this research project, the EU-funded AVERT "Aerodynamic Validation of Emission Reducing Technologies" project, coordinated by Airbus Operations Ltd, was launched in January 2007. For high-speed technologies, demonstration tests were focused on buffet control and were performed on a 3D half wing/fuselage body at the ONERA S2MA facility, in March 2010 [2]. The main characteristics of fluidic VGs and TED were defined by ONERA and LEA Poitiers [3], respectively. In parallel, ONERA pursued buffet investigations on a 3D wing, the geometry of which being similar to that of the model tested at the ONERA S2MA wind tunnel, but adapted to fit in with the test section of the "research-type" ONERA S3Ch wind tunnel [4].

Later on, within the framework of the Clean Sky SFWA-ITD "Smart Fixed Wing Aircraft – Integrated Technology Demonstrator", complementary high-speed tests were carried out on the 3D turbulent wing at the ONERA S3Ch wind tunnel in 2011, using fluidic VGs in open and closed loops. Then, in January 2012, the final demonstration of buffet closed-loop control of the BUFET'N Co project has been performed in the ONERA S2MA wind tunnel. This paper aims at providing the main outcomes from all these experimental tests.

First, the different models and their equipment will be presented. The control by passive VGs will be first presented as a reference. Then, results obtained with fluidic control by fluidic VGs (continuous and pulsed) and by fluidic TEDs will be detailed. The last section will be dedicated to the closed-loop buffet control by fluidic VGs.

2. Wind tunnel models

Before being performed in an "industrial-type" wind tunnel, tests have been carried out in the S3Ch wind tunnel of the ONERA Meudon Centre. The objective of these tests was to assess the efficiency of the fluidic VGs, by comparison with a more classical solution based on mechanical VGs. The experimental set-up is shown in Fig. 1. The model is composed of a swept wing attached on a half-fuselage with a peniche. This model was designed during the BUFET'N Co project and most of the wing is based on the supercritical OAT15A airfoil. The swept angle at the leading edge is equal to 30°. The wing twist was adapted to ensure a constant pressure along the span under cruising conditions, as well as a shock parallel to the leading edge. From root to tip, the chord varies between 240 mm and 200 mm over a span of 704 mm. In the end, no separation at the wing root was ensured using adapted profiles in that region in order to smooth the shock close to the fuselage.

Then, after these first validation tests, wind tunnel tests have been performed in the S2MA wind tunnel of the ONERA Modane–Avrieux Centre. This wind tunnel allows larger models to be tested. Moreover, it is equipped with a balance, which enables one to study the buffet onset by varying the angle of attack of the model. Fig. 2 shows the AVERT model in the S2Ma wind tunnel. The half-model geometry consists in a wing, a fuselage, and a peniche. The wing cross-section geometry is mostly based on the OAT15A airfoil, as for the S3Ch model in Fig. 1. The wing span is larger (1.225 m) and the sweep angle is the same (30°). The chord length is 0.450 m at the wing root and 0.225 m at the wing tip. The mean aerodynamic chord is 0.3375 m.

3. Buffet control by passive VGs

As explained in the introduction, the first objective was to define a reference configuration with efficient control, with which the others fluidic control devices like the fluidic VGs will be compared. It is well known that mechanical VGs are able to postpone buffet onset, so they have been chosen as a reference. Since the wing is swept, only co-rotating VGs are considered here. The VGs, whose vertices are located at 20% of the chord, consist of 27 small triangles with a height

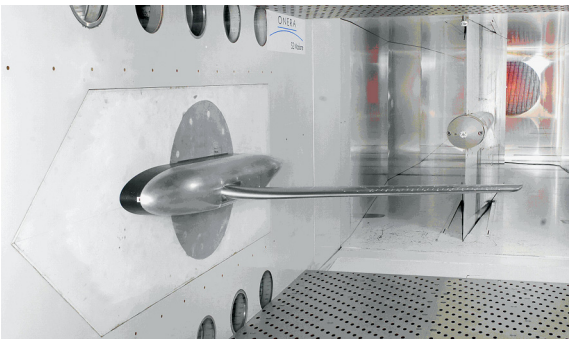

Fig. 2. The AVERT model in the S2MA wind tunnel.

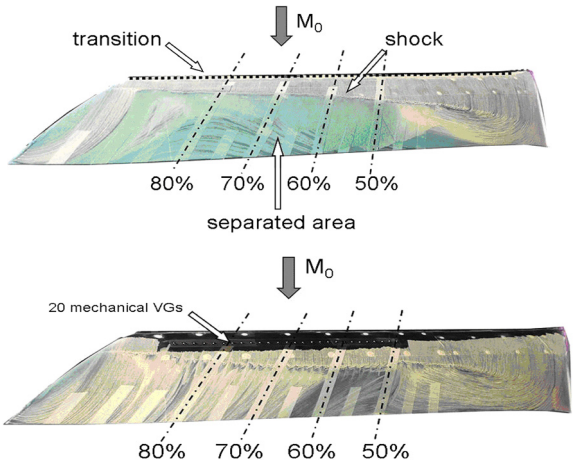

Fig. 3. (Colour online.) Oil flow visualization without control (top) and with mechanical VGs (bottom) at $y/b = 75\%$ (right) ($\alpha = 3.5°$, $M_0 = 0.82$).

$h = \delta = 1.3$ mm and a length equal to $5h$. Their skew angle has been defined using numerical simulations [5] and is equal to $\beta = 30°$ with respect to the free-stream direction (and so $\beta = 0°$ with respect to the leading edge normal). The first VG is located at 51% of the half-span (b), the last one at 89%, and the spacing between the VGs is 1.7% of the half-span ($\lambda = 12h$). Fig. 3 (bottom) shows an oil flow visualization of the controlled configurations with mechanical VGs. By comparing with the baseline without control (top), one can observe that flow separation has been suppressed over most of the wing span, except between $y/b = 0.5$ and 0.6 where a recirculation zone remains. This is due to the fact that VGs are only located between 50% and 90% of the span, which leaves the first half of the wing uncontrolled and prone to separation, like for the baseline.

4. Buffet control by fluidic VGs

4.1. Continuous blowing

On the S3Ch model, a cover with 40 co-rotating fluidic VGs has been manufactured to try to reproduce the effect of the mechanical VGs, with the advantage of being able to activate them only when they are necessary. The fluidic VGs consist in small nozzles with a conical shape and a supersonic exit flow at $M_{VG} = 2$. The exit diameter of the nozzles (d) is equal to 1 mm and the pitch angle (defined between the jet direction and the local wall tangent, see Fig. 4 (left)) is $\alpha = 30°$. The 40 continuous fluidic VGs are located between 53% and 82% of the span, with a spacing equal to 0.85% of the span ($\lambda = 6$ mm). A different cover with 25 pulsed fluidic VGs has also been manufactured. They are located at between 50% and 84% of the span with a spacing equal to 1.63% of the span ($\lambda = 11.5$ mm). The orientation of the jets with respect to the leading edge of the model β being an important parameter, it has been studied numerically (see Ref. [5]), in order to define the most promising skew angles to be tested. Thus, on the S3Ch model, two skew angles for continuous fluidic VGs have been tested: $\beta = 60°$ and 90° with respect to the free-stream direction (they are named VGF4 and VGF5 in the following, respectively) and one for the pulsed fluidic VGs: $\beta = 60°$ (named VGFp). These pulsed fluidic VGs consist in ONERA home-made piezoelectric actuators supplied with compressed air and driven by an electric square signal. They are located at 23% of the chord. More details on the pulsed fluidic VG actuator can be found in Ref. [6].

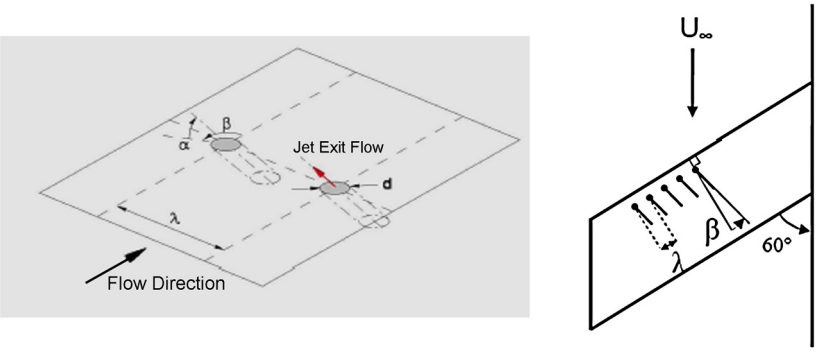

Fig. 4. The sketch showing the definitions of the main parameters of the fluidic VGs.

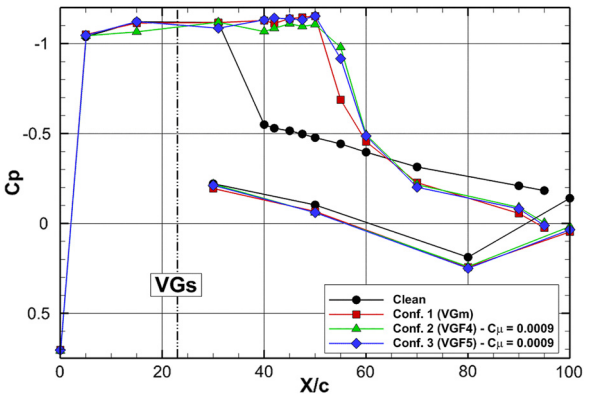

Fig. 5. (Colour online.) Effect of the fluidic VGs mass flow rate on Cp distributions at $y/b = 0.7$ (S3Ch, $\alpha = 3.5°$, $M_0 = 0.82$).

For the fluidic VGs, the momentum coefficient C_μ is defined by:

$$C_\mu = \frac{\rho_j S_j U_j^2}{\frac{1}{2}\rho_0 S U_0^2} = \frac{q_m U_j}{\frac{1}{2}\rho_0 S U_0^2}$$

where ρ_j and U_j are respectively the density and velocity of the jets (time-averaged in the pulsed blowing case), S_j the sum of all of the orifice surface area based on the hole diameter (not the projected surface) and q_m is the mass flow rate (time-averaged in the pulsed blowing case). When the flow at the exit of the nozzles is supersonic, the Mach number ($M = 2$) and thus U_j are fixed and only the mass flow rate continues to increase with the air supply stagnation pressure. The variables ρ_0 and U_0 are, respectively, the free-stream density and velocity of the main flow, the wing surface corresponding to a half span being denoted by S.

Fig. 5 shows a comparison of the Cp distributions at $y/b = 0.7$ between the baseline, mechanical and fluidic VGs configurations in strong buffet conditions. The results show that the control effect on the pressure plateau level upstream of the shock is negligible. The shock location has been shifted more downstream on the wing at around $X/c = 0.55$, because of the separation size reduction for all controlled cases. The shock seems to be located slightly more downstream in the fluidic VGs case than for the mechanical VGs. For this value of the momentum coefficient C_μ, which corresponds to a saturated effect of the fluidic VGs, the skew angle β seems to have no effect on the wall pressure distribution.

The RMS pressure chordwise distributions at $y/b = 0.6$ (only section equipped with Kulite sensors on this model) of the clean and controlled configurations are compared in Fig. 6. For the three controlled configurations, the maximum level corresponding to the crossing of the shock is located at about $X/c = 0.55$. More downstream, the pressure fluctuation levels are lower than for the baseline in all controlled cases. This confirms that unsteadiness in the separated region has been damped with either passive or active control. One can also note that the lowest levels are obtained by fluidic VGs. However, pressure fluctuation levels at the shock location are greater in the controlled cases than for the baseline, because the shock is located between two sensors for the baseline (see the shock position in Fig. 6) and consequently the peak is not visible in the figure.

Fig. 7 shows the effect of comparison of acceleration levels between the baseline and the controlled configurations with mechanical and fluidic VGs. In all controlled cases, the vibration level has been drastically reduced compared to the uncontrolled one. Mechanical and both tested fluidic VG configurations exhibit the same level of acceleration.

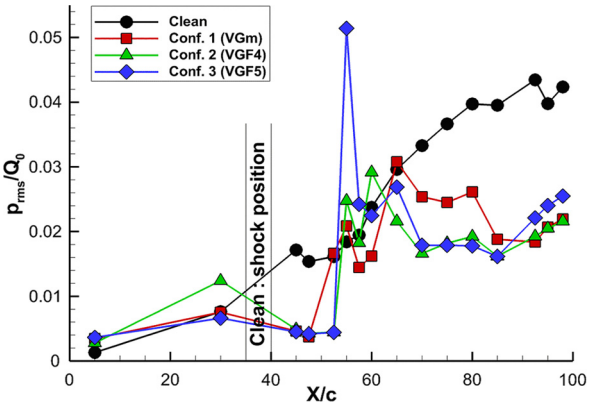

Fig. 6. (Colour online.) Comparison of RMS pressure distributions at $y/b = 0.6$ ($\alpha = 3.5°$, $M_0 = 0.82$).

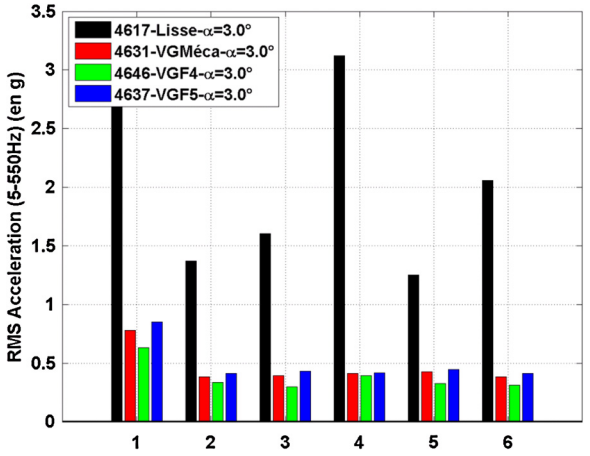

Fig. 7. (Colour online.) Comparison of acceleration levels on the six accelerometers ($\alpha = 3°$, $M_0 = 0.82$).

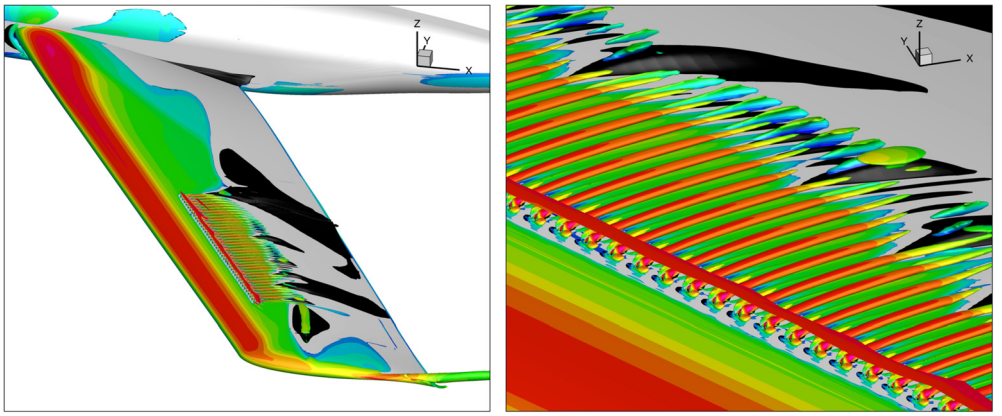

Fig. 8. (Colour online.) Q-criterion isosurface ($Q = 100U_\infty^2/h^2$) coloured by the Mach number and separated zone (in black) showing the streamwise vortices created by the co-rotating fluidic VGs.

This test case has been computed with the ***elsA*** software by Dandois et al. [5]. Fig. 8 displays a Q-criterion isosurface ($Q = 100U_\infty^2/h^2$) coloured by the Mach number and the isosurface $Vx = 0$ (streamwise velocity $= 0$, in black) for the fine overset grid. The streamwise vortices created by the co-rotating fluidic VGs are clearly visible. As observed in the experiment, there remains a small separated zone between 50% and 60% of the span.

Concerning the S2MA model, like for the S3Ch model, micro-nozzles with a throat diameter of 0.8 mm and an exit diameter $d = 1$ mm have been used. Since the model is larger than the S3Ch one, there are 50 fluidic VGs instead of 40. They are also located closer to the leading edge at 15% of the chord, in order to be outside the fuel tank region on a real

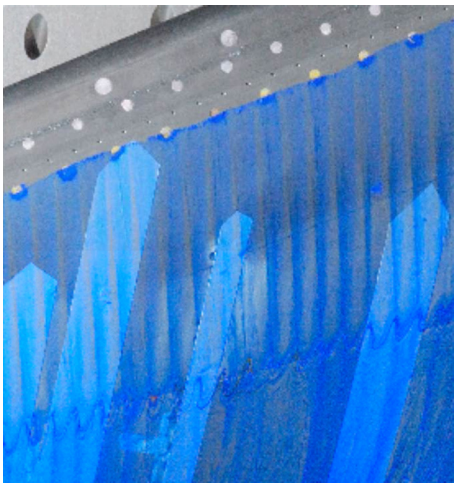

Fig. 9. (Colour online.) Close-up view of the oil flow visualization around the fluidic VGs at $\alpha = 3^\circ$ and $C_\mu = 5.8 \times 10^{-4}$ (S2MA, $M = 0.82$, $Re_c = 2.83 \times 10^6$).

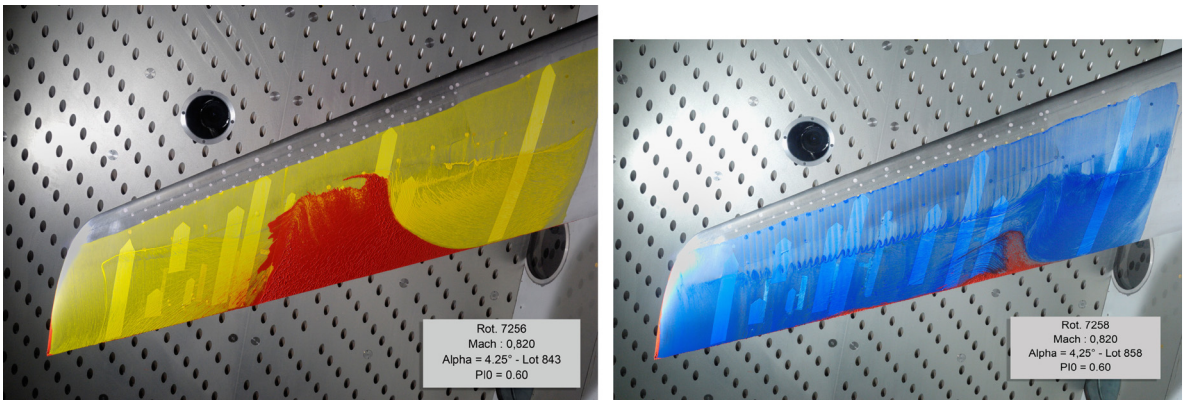

Fig. 10. (Colour online.) Oil flow visualizations of the baseline (left) and the fluidic VGs case ($C_\mu = 5.8 \times 10^{-4}$) at $\alpha = 4.25^\circ$.

aircraft. They are located between 46% and 89% of the wing span. The spacing between each hole is $\lambda = 14.4d$. Like for the S3Ch model, the pitch angle α is fixed equal to 30°. Since on the S3Ch model no difference was observed between the two tested skew angles, only $\beta = 90^\circ$ (with respect to the free-stream direction) has been tested on this model. The maximum mass flow is $0.5\ \mathrm{g \cdot s^{-1}}$ per hole and the fluidic VGs can operate in continuous blowing mode, or in pulsed blowing mode (between 0 Hz and 700 Hz) using piezoelectric actuators inside the model. Fig. 9 shows a close-up view of the oil flow visualization of the controlled flow by fluidic VGs ($C_\mu = 5.8 \times 10^{-4}$) at $\alpha = 3^\circ$ i.e. at buffet onset conditions. The streamwise vortices created by the VGs are traced by the streamwise line of oil washing between accumulations of blue oil. The shock foot is also modified by the interaction with the streamwise vortices. For a higher angle of attack in strong buffet $\alpha = 4.25^\circ$ (see Fig. 10), in the uncontrolled case, the flow is separated on one third of the span in the central part, whereas in the controlled case with fluidic VGs, a flow separation starts to appear at around 40% of the span where the flow is not controlled (the fluidic VGs are located between 46% and 89% of the span). Thus, the fluidic VGs are able to delay the separation appearance as well as the mechanical VGs.

Since the S2MA wind tunnel is equipped with a balance, the effect of the fluidic VGs on lift and drag can be investigated. The lift evolution with the angle of attack is given in Fig. 11 for the baseline, the mechanical VGs case and the fluidic VGs for some selected values of C_μ. The control has no influence on the lift curves for $\alpha < 2.5^\circ$. For $\alpha > 2.5^\circ$, the lift curves of the baseline and the controlled case start to diverge, the control increases the lift. Then, for $\alpha > 4^\circ$, the lift increment is nearly constant. The lift increment, observed for angles of attack larger than the buffet onset at $\alpha = 3^\circ$, increases with C_μ, but quickly reaches a saturation for $C_\mu \geq 4.6 \times 10^{-4}$, which corresponds to a low value C_μ (5% of the maximum C_μ) and of the mass flow rate ($5.9\ \mathrm{g \cdot s^{-1}} = 1/4$ of the maximum mass flow rate). The micro-nozzles are not even shocked. Fig. 11 shows that the lift curves for $C_\mu = 4.6 \times 10^{-4}$ and 1.7×10^{-3} are superimposed. The effect of the fluidic VGs on lift is comparable to the mechanical VGs one for a very low value of C_μ equal to 1.5×10^{-4} ($3\ \mathrm{g \cdot s^{-1}}$).

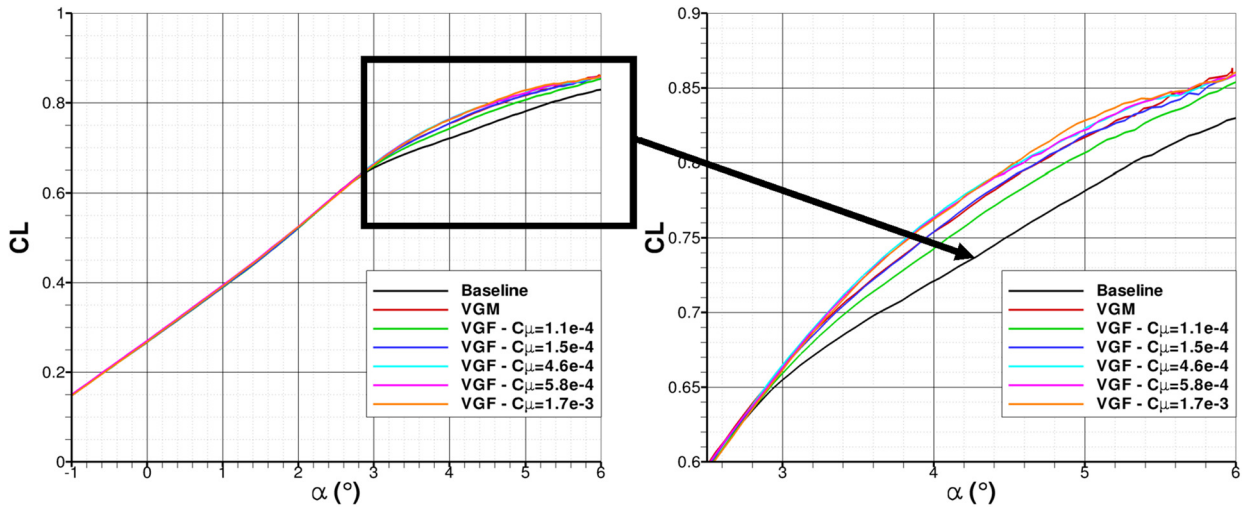

Fig. 11. (Colour online.) Lift change with the angle of attack for the baseline, the mechanical VGs and some selected fluidic VGs cases ($M = 0.82$, $Re_c = 2.83 \times 10^6$).

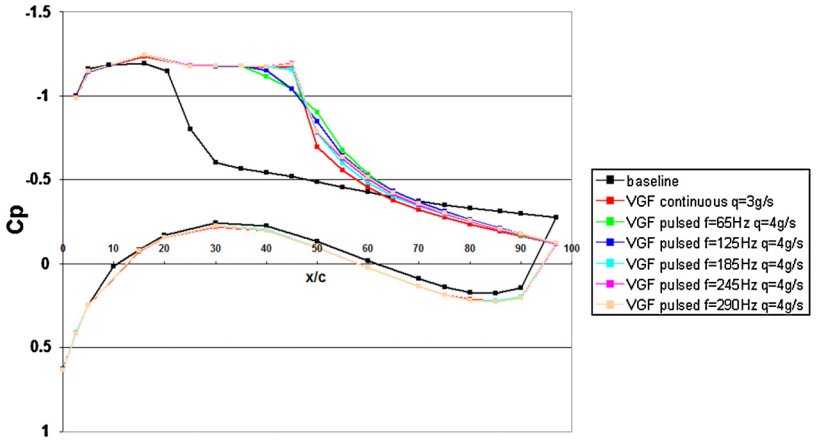

Fig. 12. (Colour online.) Wall pressure distribution for the baseline, continuous blowing fluidic VGs and pulsed fluidic VGs at $\alpha = 4.25°$ and different frequencies at 4 $g \cdot s^{-1}$ (S2MA).

4.2. Pulsed blowing

The wall pressure distributions for the baseline, the continuous blowing VGs and the pulsed fluidic VGs case at a mass flow rate of 4 $g \cdot s^{-1}$ ($C_\mu = 3 \times 10^{-4}$) are given in Fig. 12 for an angle-of-attack of 4.25° and $y/b = 72.5\%$. The actuator command varies between 0% and 100% of the fluidic VGs opening. As for the continuous blowing fluidic VGs, the effect of the pulsed fluidic VGs is to suppress the flow separation characterized by the Cp increase at the trailing edge, which occurs for $\alpha \geq 3°$ for the baseline and to shift the shock downstream. The effect of the forcing frequency of the pulsed fluidic VGs is to modify the Cp gradient at the shock foot at around 50% of the chord: for $f = 65$ Hz and 125 Hz, this gradient is smaller than in the continuous blowing case and than that for pulsed fluidic VGs with $f \geq 185$ Hz. This lower Cp gradient characterizes, in 2D, the shock motion on the suction of the airfoil so here, for a forcing frequency of 65 and 125 Hz, the shock motion amplitude is increased compared to the baseline.

5. Buffet control by fluidic TED

The fluidic TED consists in a slot located on the lower side of the model at the trailing edge. The blowing angle is normal to the lower surface (see Fig. 13). Its design is similar to that developed by LEA [3] for the VZLU WT tests during the AVERT European project. The slot is located at $x/c = 95\%$ and its width is equal to 0.5 mm. The spanwise length of the slot is 490 mm (between 45% and 85% of wing span). The design of the plenum that supplies the slot with air is based on the TED design for VZLU tests: four transverse sections can be feed separately, the maximum mass flow being equal to 180 $g \cdot s^{-1}$ (4×45 $g \cdot s^{-1}$, $C_\mu = 9 \times 10^{-3}$).

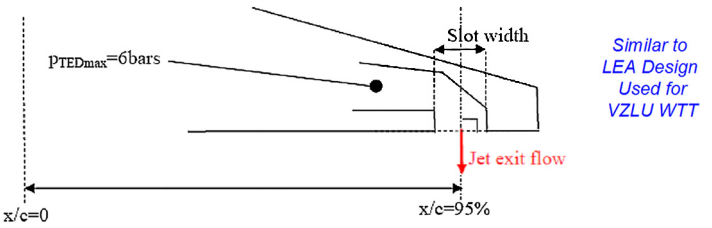

Fig. 13. (Colour online.) Sketch showing the definitions of the main parameters of the fluidic TED.

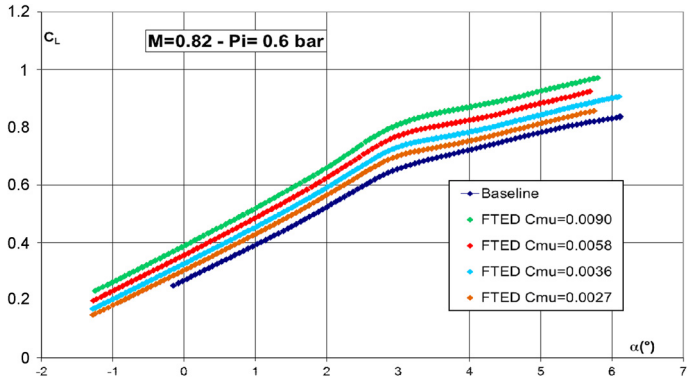

Fig. 14. (Colour online.) Fluidic TED action (up to the maximal value of the blowing mass flow rate) on the lift versus α (S2MA, $M = 0.82$, $Re_c = 2.83 \times 10^6$).

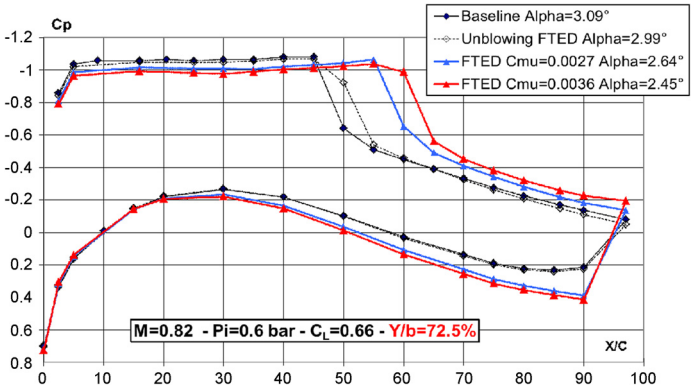

Fig. 15. (Colour online.) Wall pressure distributions ($M = 0.82$, $Re_c = 2.83 \times 10^6$): increasing fluidic TED effect at a constant value of the lift coefficient $C_L = 0.66$ corresponding to buffet onset.

The lift change with the angle-of-attack is given in Fig. 14. The effect of the fluidic TED is a constant increase in its value over the entire angle-of-attack range. This global variation on C_L is progressive with the increase of the C_μ. Up to the maximal value of C_μ (0.0090), corresponding to the maximal mass flow rate of the test device, the observed effects vary linearly with C_μ: the effect for $C_\mu = 0.0090$ is approximately three times that for $C_\mu = 0.0027$.

The static wall pressure distributions for the baseline and the fluidic TED are given in Fig. 15 for different C_μ values at the same lift coefficient value. This constant lift coefficient value of 0.66 corresponds to the buffet appearance for the baseline configuration ($\alpha \sim 3°$). When the fluidic TED slot is not blowing (slot open–dashed line), there are only slight differences in the pressure distributions compared to the baseline configuration case. When the fluidic TED slot is blowing, the strong upper side shock wave moves downstream (10% to 15% of the chord), while the wide supersonic plateau upstream of it becomes lower. On the aft part of the wing, the rear loading is increased.

6. Summary of open-loop results

Fig. 16 summarizes the behaviour concerning buffet onset and development for the mechanical and fluidic VG configurations, in comparison with the baseline configuration at $M = 0.82$ and $Re_c = 2.83 \times 10^6$. The RMS fluctuations values are plotted versus the angle of attack and versus the lift coefficient for the upper side Kulite pressure transducer named K2, located near the trailing edge at $x/c = 85\%$ on the spanwise section $y/b = 75\%$.

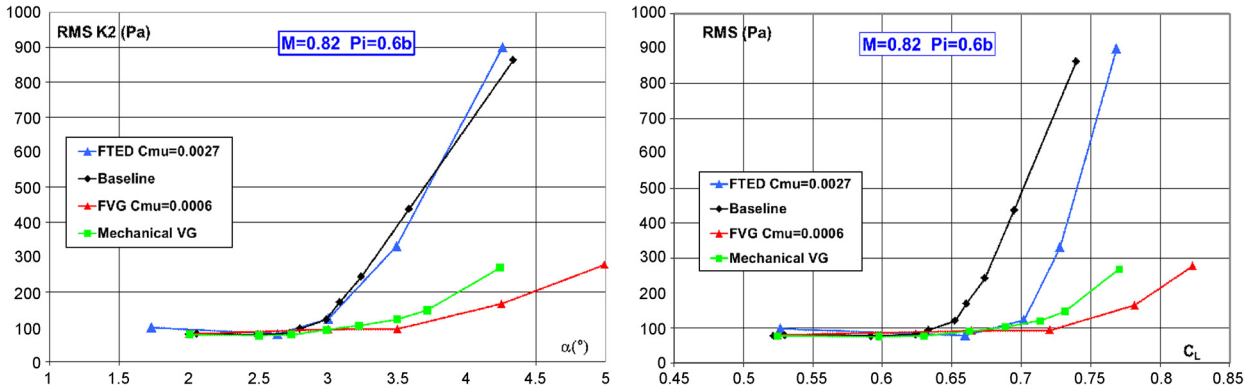

Fig. 16. (Colour online.) Buffet entrance with fluidic and mechanical VGs; comparison with the baseline configuration at $M = 0.82$ and $Re_c = 2.83 \times 10^6$: unsteady wall pressure measurements.

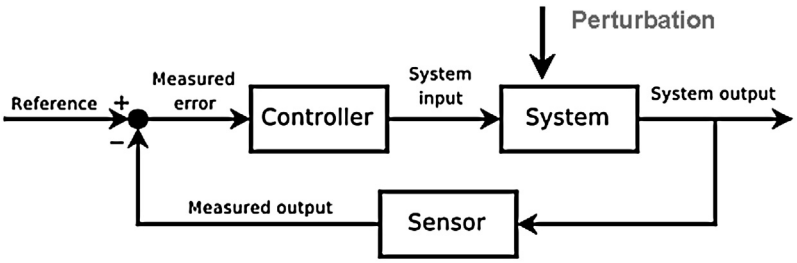

Fig. 17. Principle scheme of feedback control.

At low values of α or lift coefficient, fluidic or mechanical VGs do not produce any increase of the mechanical vibration level. For mechanical VGs, the strong increase in the pressure fluctuation and mechanical vibration corresponding to buffet is clearly postponed to higher angle-of-attack and lift values. Moreover, the increase in the pressure fluctuation seems to be reduced when buffet becomes stronger. The buffet onset limit is estimated at $\alpha = 3°$ (instead of 2.75° for the baseline). For fluidic VGs, the effects are similar, but stronger. At $C_\mu = 0.0006$, the buffet onset limit can be estimated at $\alpha = 3.25°$ and the increase in the pressure fluctuation when buffet develops is lower, as for the baseline or even the mechanical VGs configuration.

Concerning the control by the fluidic TED, it is important to note that this flow control device does not delay the buffet onset at higher angles of attack (see Fig. 16 (left)) but only at higher lift values (see Fig. 16 (right)) since, as was shown in Fig. 14, the effect is a constant lift increase over the entire angle-of-attack range and the kink visible on the lift curve at around 3° is not delayed by the fluidic TED.

7. Closed-loop control by fluidic VGs

7.1. The quasi-static approach

The general principle of a classical feedback loop is represented in Fig. 17. The output of the system observed by the sensors is compared to the reference input and the error signal is passed into a controller and applied to the system. The design problem consists in finding the appropriate controller such that the closed-loop system is stable and behaves according to the specifications.

The application of a feedback control for buffet phenomena alleviation can be associated with a disturbance rejection strategy. In this case, no reference input is applied to the system, the control architecture aims at minimizing its response to a specific perturbation. For the proposed closed-loop approach, the quasi-steadiness property results from the fact that the system output is passed into an integrator block in order to estimate a specific criterion (RMS value, averaged value) over a “long time” (a few seconds). The main control parameters are described in Table 1 and depend on the signal and the objective function used in the closed loop.

The two lines of Table 1 correspond to two different strategies. The first one is based on the signal of an unsteady pressure sensor located near the trailing edge. The use of these data in the feedback loop leads to an action on the flow separation phenomena in the sensor area. The second strategy is based on a shock location signal and should allow an effect on the shock wave instability phenomena. The two closed loop control architectures were first tested in the S3Ch wind tunnel for a unique aerodynamic condition: $M = 0.82$, $Re_c = 2.5 \times 10^6$ and angle of attack of 3° (close to buffet onset). Moreover, for each case, the feedback gain was tuned manually.

Table 1
Control configurations tested during WT test campaign.

Sensor	Criterion	
	RMS value	Mean value
Trailing edge pressure signal	Minimization	Maximization
Shock location signal	Minimization	Maximization

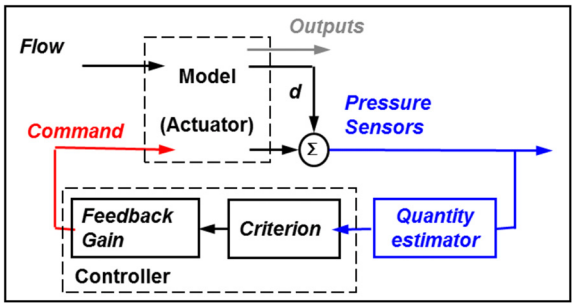

Fig. 18. (Colour online.) Bloc diagram of the buffet control loop.

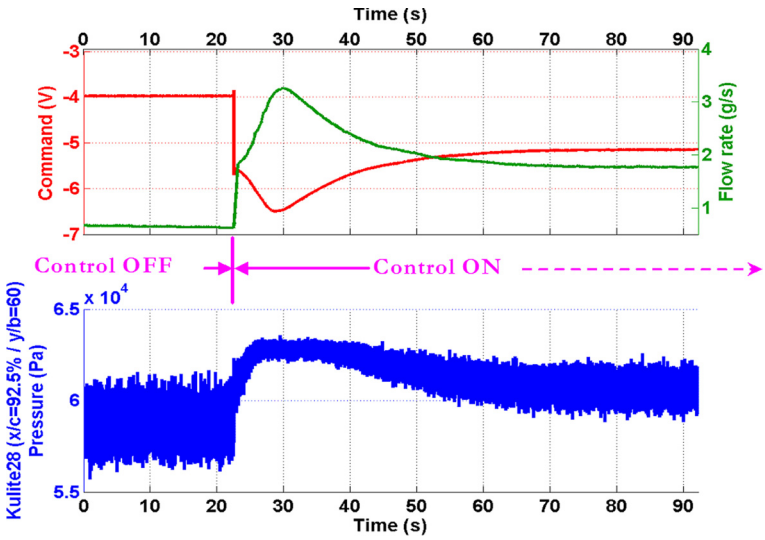

Fig. 19. (Colour online.) Time evolutions of command, flow rate and pressure signal.

7.2. Real-time control system

All closed-loop strategies have been implemented by Onera on a real time dSPACE device which comprises several processors and input/output boards interlinked for fast internal communication and data exchange. The I/O interface is composed of a maximum of 15 analogue inputs and 18 analogue outputs. A dedicated computer is used for creating, compiling and implementing Simulink models in the processor boards and a real-time man/machine interface has been developed to monitor the signals and change control/command parameters.

The schematic control architecture is shown in Fig. 18. The control laws are based on unsteady pressure data and used in a SISO configuration (i.e. Single Input Single Output) or MISO (i.e. Multi Input Single Output). All fluidic VGs are therefore driven synchronously by a unique command signal.

7.3. Quasi-steady control of the RMS value of a trailing edge unsteady pressure sensor

The main results are plotted in Figs. 19 and 20. Starting from the uncontrolled configuration, the pressure fluctuations level (estimated through the RMS value) is very high. The command of the fluidic VG is determined proportionally to this signal through the closed loop. As the efficiency of the control modified the signal RMS value, the leading actuation command is adjusted in the same way. After a rise time and a settling time, the control command converged to a fixed value.

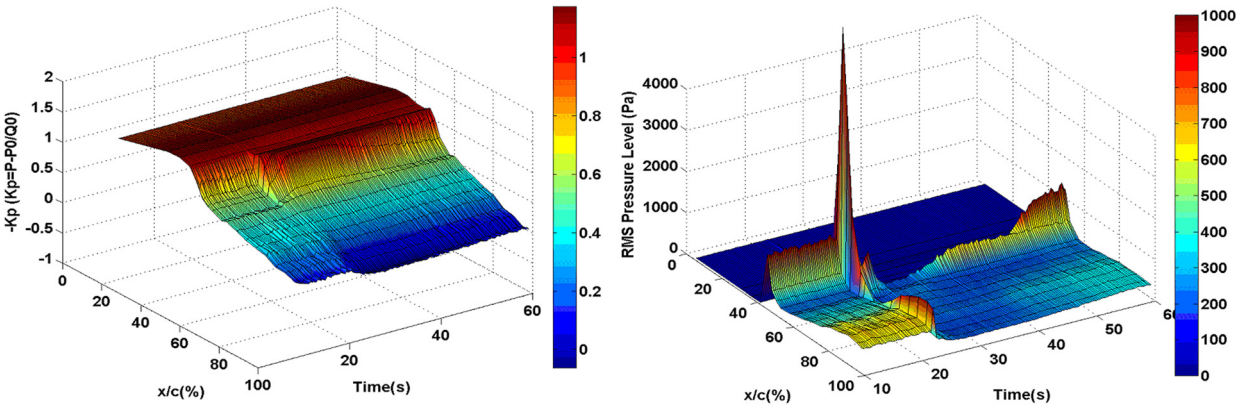

Fig. 20. (Colour online.) Pressure coefficient distribution (left) and RMS value distribution (right) at $y/b = 60\%$.

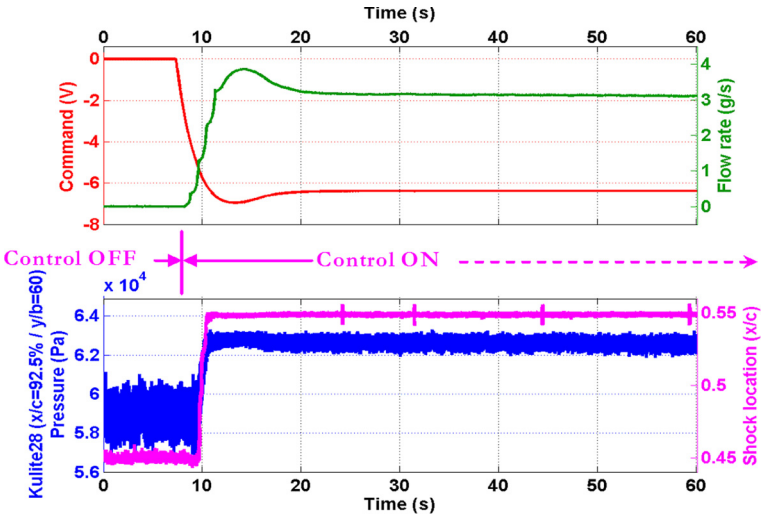

Fig. 21. (Colour online.) Time evolution of command, flow rate, pressure and shock-location signals.

The temporal evolutions of the wall pressure distributions ($-K_p$ and RMS) along the chord located at $y/b = 60\%$ are detailed in Fig. 20. The closed loop is activated at $t = 20$ s. After a transient state, the reduction of the RMS value of the unsteady pressure fluctuations is clearly visible at the trailing edge, indicating that the flow separation has been suppressed. At the same time, pressure coefficient and RMS distributions indicated that the shock location moved more downstream.

The transient state, observed after the control has been switched on, coincided with the conclusions of cases with low flow rate [5]. Previous tests performed with continuous flow rate indicated that, for low momentum coefficient values, the action of fluidic VG actuators on buffet could be the opposite of the desired effect: increase of RMS pressure levels, expansion of the flow detachment…

7.4. Quasi-steady control of the averaged value of a "shock location sensor"

In this second approach, 10 unsteady pressure sensors are monitored continuously in order to estimate the shock location. The function of the "quantity estimator block" (see Fig. 18) is to estimate the shock location in real time. The resulting signal is used as an input of the controller. The objective is move the shock downstream since, as shown by Fig. 5, it will result in the flow separation suppression. The main results are plotted in Fig. 21. As in the previous case, the evolution of the fluidic VG command is clearly proportional to the chosen signal. With a small gain value, the actual command may result to an inefficient fluidic VG command or can converge to the desirable output slowly. However, with a large control gain, the actual output can reach the (maximum) saturation value or may never converge (i.e. the controller-plant system oscillates). At the end of the test point, the control efficiency is proved by the fact that the shock location has moved 10% of chord downstream. The RMS fluctuations of shock location (but also of the unsteady pressure at the trailing edge) are clearly decreased.

8. Conclusion

The aim of this paper was to summarize the work performed at ONERA over the last six years within the framework of several European and self-funded projects. The efficiency of flow control devices has been evaluated in two wind tunnels under transonic flow conditions, at different Mach and Reynolds numbers. These results, recorded in an industrial-type environment, have allowed the behaviour of such active technologies to be assessed and to be brought to TRL "Technology Readiness Level" values of 3–4. To summarize the results, the effects of both passive and active devices are to:

- postpone buffet onset at a higher angles of attack (mechanical/fluidic VGs), or at higher lift values (all);
- decrease the extent of separated areas (from oil-flow visualizations);
- decrease the unsteadiness (records provided by Kulite transducers and accelerometers);
- increase the lift coefficient at high angles of attack (from force measurements).

Many parametric investigations were performed (not all shown here) for different fluidic VG spacings, spanwise locations and also mass flow rates, and thus momentum coefficients.

The effect of the fluidic VGs is similar to that of the mechanical VGs, with a saturation reached for a momentum coefficient C_μ above 9×10^{-5}, corresponding to a flow rate of $0.12\ g \cdot s^{-1}$ per hole. Fluidic VGs at C_μ of 6×10^{-5} have very similar aerodynamic performances to those of the mechanical VGs case. The effect on unsteady components is very similar. Concerning the fluidic TED, linear-type behaviour has been noted on the lift coefficient. It should be pointed out that the efficiency of a fluidic TED with $C_\mu = 0.0027$ corresponds to that of a mechanical TED or mini-flap deflected at $\sim 30°$ when comparing to former results obtained by ONERA.

The closed-loop control using fluidic VGs has demonstrated the feasibility of controlling the buffet using a quasi-steady approach. Different control laws have been developed to adjust the actuators mass flow rate thanks to a feedback command based on the real time estimation of the shock location or the flow separation level (RMS of pressure).

Acknowledgements

The AVERT wind tunnel tests were conducted within the FP7 AVERT European project (Contract No. AST5-CT-2006-030914), funded by EC and project partners (Airbus Operations Ltd, Airbus Operations SL, Dassault Aviation, Alenia Aeronautica, and ONERA). The closed-loop buffet control tests in the S3Ch wind tunnel, as well as the synthetic jet tests in the S2MA wind tunnel, have received funding from the European Union's Seventh Framework Program (FP7/2007–2013) for the Clean Sky Joint Technology Initiative, under Grant Agreement CSJU-GAM-SFWA-2008-001. The authors are very grateful to the ONERA S3Ch and S2MA wind tunnel teams, who contributed to the success of these tests.

References

[1] É. Coustols, V. Brunet, R. Bur, D. Caruana, D. Sipp, BUFET'N Co: a joint ONERA research project devoted to buffet control on a transonic 3D wing using a closed-loop approach, in: CEAS/KATNET II Conference, Bremen, Germany, 2009.
[2] J. Dandois, P. Molton, A. Lepage, A. Geeraert, V. Brunet, J.-B. Dor, É. Coustols, Buffet characterisation and control for turbulent wings, Aerosp. Lab. J. 6 (2013), http://www.aerospacelab-journal.org.
[3] G. Browaeys, H. Deniau, E. Collin, J.-P. Bonnet, Pneumatic control strategies for transonic buffet. A numerical approach, in: 7th International Symposium on Engineering Turbulence Modeling and Measurement (ETMM7), Limassol, Cyprus, 2008.
[4] P. Molton, J. Dandois, A. Lepage, V. Brunet, R. Bur, Control of buffet phenomenon on a transonic swept wing, AIAA J. 51 (4) (2013) 761–772.
[5] J. Dandois, V. Brunet, P. Molton, J.-C. Abart, A. Lepage, Buffet control by means of mechanical and fluidic vortex generators, AIAA paper 2010-4975, in: 5th AIAA Flow Control Conference, Chicago, IL, 2010.
[6] F. Ternoy, J. Dandois, F. David, M. Pruvost, Overview of ONERA actuators for active flow control, Aerosp. Lab. J. 6 (2013), http://www.aerospacelab-journal.org.